Proceedings of ASME Turbo Expo 2011
GT2011
June 6-10, 2011, Vancouver, British Columbia, Canada

GT2011-46744

MIXTURE-FORCED FLAME TRANSFER FUNCTION MEASUREMENTS AND MECHANISMS IN A SINGLE-NOZZLE COMBUSTOR AT ELEVATED PRESSURE

Nick Bunce, Jong Guen Lee, Bryan D. Quay, and Domenic A. Santavicca
Department of Mechanical and Nuclear Engineering
Center for Advanced Power Generation
The Pennsylvania State University, University Park, PA, 16802

ABSTRACT

The mixture-forced flame transfer function of a lean fully premixed single-nozzle research combustor operating on natural gas is determined experimentally at combustor pressures from 1 to 4 atm. Measurements are made over a range of inlet temperatures (100-300°C), mean velocities (25-35 m/s), and equivalence ratios (0.5-0.75). A rotating siren device, located upstream of the nozzle, is used to modulate the flow rate of the premixed fuel-air mixture. The amplitude and phase of the resultant velocity fluctuation are measured near the exit of the nozzle using the two-microphone method. The measured normalized velocity fluctuation serves as the input to the flame transfer function. In this study, the amplitude of the normalized velocity fluctuation is fixed at 5% and the modulation frequency is varied from 100 to 500 Hz. The output of the flame transfer function is the normalized global heat release fluctuation, which is measured using a photomultiplier tube and interference filter which captures the CH* chemiluminescence from the entire flame. In addition, two-dimensional CH* chemiluminescence images are taken for both forced and unforced flames. Forced flame images are phase-synchronized with the velocity fluctuation. The flame transfer functions for all of the operating conditions tested exhibit similar behavior. At low frequencies, the gain is initially greater than one, but then decreases as the frequency increases. After reaching a minimum, the gain increases with increasing frequency to a second peak and then again decreases. At certain operating conditions, the gain exhibits a second minimum. At frequencies corresponding to the minima in gain the phase curve exhibits inflection points. Regions of maximum and minimum gain are explained in terms of the constructive and destructive interference of vorticity fluctuations generated in the inner and outer shear layers. Phase-synchronized images are analyzed to isolate the fluctuating component of heat release. At frequencies where the gain is amplified, this analysis shows that the heat release fluctuations caused by the vorticity fluctuations generated in the inner and outer shear layers are in phase. While when the gain is at its minimum value, the heat release fluctuations are out of phase and therefore destructively interfere.

INTRODUCTION

Due to ever more stringent emissions standards, power generation gas turbines have transitioned to lean-premixed combustion from diffusion combustion. Although this transition translates into greatly reduced emissions of pollutant species such as NO_x, it also increases the system's susceptibility to self-excited combustion instabilities [1, 2]. Combustion instabilities result from the coupling between unsteady heat release from the flame and system acoustics which lead to sustained large amplitude pressure oscillations in the combustor. Detrimental consequences of combustion instabilities include decreased overall system efficiency and severe damage to system components. Unsteady heat release can be caused by inlet velocity fluctuations and/or equivalence ratio fluctuations. In a fully premixed system the air and fuel are mixed upstream of a choked inlet to eliminate the possibility of equivalence ratio fluctuations. Therefore velocity fluctuations are the cause of heat release fluctuations in the self-excited combustion instability feedback loop under fully premixed conditions illustrated in Figure 1.

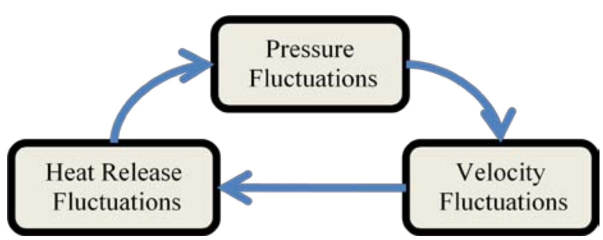

Figure 1 Self-excited combustion instability feedback loop under fully premixed conditions

In order to predict combustion instabilities during the design stage an analytical model of the flame's response to flow disturbances is necessary. The flame's response to inlet velocity fluctuations is expressed in terms of a flame transfer function (FTF), as a function of frequency f and amplitude A, which relates the normalized fluctuations in heat release $(Q'(f)/Q_{mean})$ and the normalized fluctuations in inlet velocity $(V'(f)/V_{mean})$, as shown in Eq. (1).

$$FTF_v(f,A) = \frac{Q^{'}(f)/Q_{mean}}{V(f)'/V_{mean}} \tag{1}$$

FTFs have been obtained theoretically [3, 4] numerically [5], and experimentally [3, 5-9]. The earliest work focused on simple laminar conical or V flames at atmospheric pressure. Although these configurations are far less complex than the turbulent, swirling, high pressure flames found in actual gas turbine combustors, they provide valuable insight into the fundamentals of understanding the flame's response to flow perturbations. Fleifil et al. [10] determined that the flame is more sensitive to low frequency perturbations than to high frequency perturbations. Two parameters affecting the flame response, a reduced frequency and the flame angle with respect to the flow direction, were identified by Schuller et al. [11]. Lieuwen [12] found that in addition to a reduced frequency and a parameter related to the flame angle, the shape of the unperturbed flame also had an effect on the flame's response.

Recent studies have focused on more realistic gas turbine configurations by investigating the response of turbulent swirling flames. Theoretical work by Preetham and Lieuwen [13] showed that the response of turbulent fully premixed flames to harmonic forcing is qualitatively similar to that of laminar fully premixed flames with significant quantitative differences. Background turbulent fluctuations were found to enhance the destruction rate of the harmonic wrinkles caused by the velocity perturbation which lead to an overall decrease in the flame area fluctuation relative to the laminar case. Kim et al. [8] experimentally measured general low-pass filter behavior in terms of gain and linear behavior in terms of phase of a turbulent, lean fully premixed, swirl-stabilized flame. Palies et al. [9] and Jones et al. [6] have most recently investigated the mechanisms through which velocity fluctuations cause heat release fluctuations in turbulent, lean-fully premixed, swirl-stabilized flames. Both studies reported amplification and damping of the flame's response in certain frequency ranges and sought to explain these phenomena by the constructive/destructive interference of two mechanisms perturbing the flame. These mechanisms will be further discussed in the "Flame Response Mechanisms" section of this paper.

One factor that all of the aforementioned research shares is that the work was done at atmospheric pressure. In reality combustors in land-based gas turbines operate at pressures on the order of 25 atmospheres. There have been few reported investigations of the FTF at elevated combustor pressure. One study does not systematically evaluate the effect of pressure [14]. The second is related to liquid fuel partially premixed aero-turbines and shows qualitative agreement between the low pressure and high pressure tests but cautions drawing further conclusions based on the limited amount of data [15]. The third notes major changes in the FTF for increasing combustor pressure [16]. Changing combustor pressure was found to change the frequencies at which the flame amplified flow disturbances which indicates that pressure has an effect on combustor stability. This fact calls into question the validity of incorporating FTF measurements made at atmospheric pressure into analytical models used to predict the stability characteristics of combustors at full engine pressure.

The objectives of this paper are:

- To experimentally measure the mixture-forced FTF of an industry scale, lean fully premixed, swirl-stabilized nozzle at elevated pressure.
- To identify the mechanism(s) through which velocity fluctuations cause heat release fluctuations and quantify their effects.

EXPERIMENTAL METHODS

The lean fully premixed, swirl-stabilized, single-nozzle gas turbine combustor used in this study consists of a siren device, nozzle, combustion chamber, and exhaust as shown in Figure 2. Premixed fuel and air enter the experiment after passing through a choked inlet to eliminate the possibility of equivalence ratio fluctuations. At this point the flow path splits and a portion of the mixture enters the siren device while the rest of the mixture bypasses it. The siren device is composed of a stator and rotor driven by a variable-speed DC motor. Velocity fluctuations are generated with this device at frequencies up to 500 Hz and amplitudes up to 45% of the mean velocity by adjusting the fraction of the fuel-air mixture which passes through the siren device and that which bypasses it. The next section is an industry scale swirl stabilized nozzle. The nozzle consists of an outer tube and inner centerbody, recessed from the dump plane, held in place by an axial swirler. Dimensions of the nozzle and combustor can be found in Fig. 3. After the nozzle is the combustion chamber, consisting of a quartz cylinder enclosed in a stainless steel box with quartz windows on two sides to allow optical access to the flame. Air is passed though the space between the outside of the cylinder and the inside of the box to both cool and minimize the pressure difference across the quartz cylinder. The last section of the experiment is the exhaust which consists of a 911 mm long 102 mm diameter stainless steel pipe with a valve at the end to allow pressurization of the combustor.

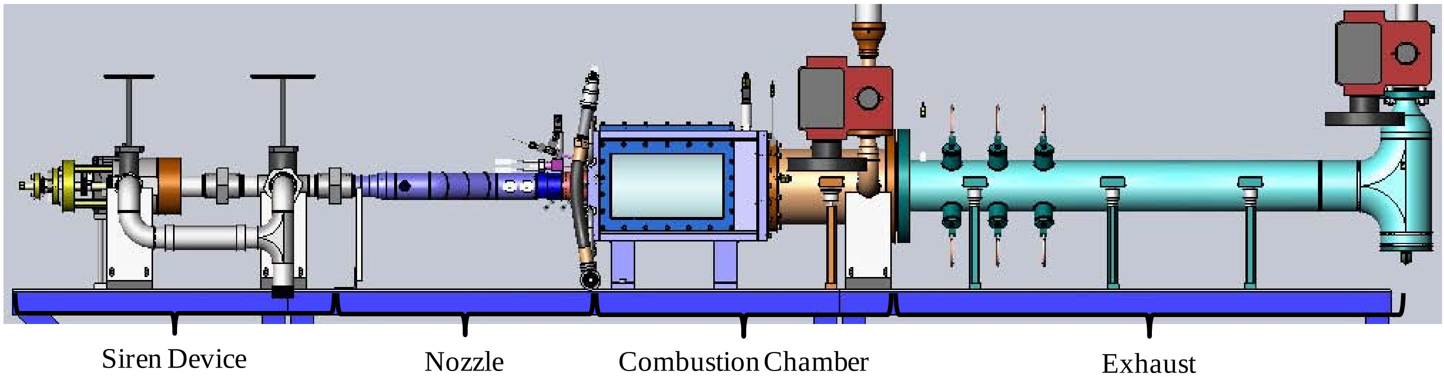

Figure 2 Schematic drawing of lean fully premixed, swirl-stabilized single-nozzle gas turbine combustor

Measurement instruments include dynamic pressure transducers (PCB model 112A05), photomultiplier tubes (Hamamatsu model H7732-10), and an intensified CCD camera (Princeton Instruments model PI-MAX). The pressure signals from two dynamic pressure transducers located 52 and 90 mm upstream of the dump plane are used to calculate the velocity fluctuation in the nozzle using the two-microphone method [17]. Three photomultiplier tubes with narrow band-pass filters are used to measure flame chemiluminescence emission from CH* (432 ± 5 nm), OH* (307 ± 5 nm), and CO_2 (365 ± 5 nm). It has been shown that under fully premixed conditions, as is the case for this study, the chemiluminescence emission intensity provides a measure of the heat release rate of the flame [18]. A National Instruments data acquisition board (model BNC-2110) in conjunction with a LabVIEW program is used to acquire the pressure and chemiluminescence signals with 8192 data points at a sampling frequency of 8192 Hz yielding a frequency resolution of 1 Hz. The fluctuating components of the signals at the forcing frequency are extracted by applying a FFT to the signals. The ICCD camera equipped with a CH* (430 ± 5 nm) band-pass filter is used to take both time-averaged images of unforced flames and phase-synchronized images of forced flames. The velocity fluctuation calculated from the two-microphone method serves as the reference signal for the phase-synchronized images. Images are taken in 30 degree increments through one period of the velocity fluctuation which gives a total of twelve images per forcing period comprising 60 accumulations each. Since the images are integrated line-of-sight images, a three point Abel deconvolution scheme is applied to extract two-dimensional flame structure information from these images [19].

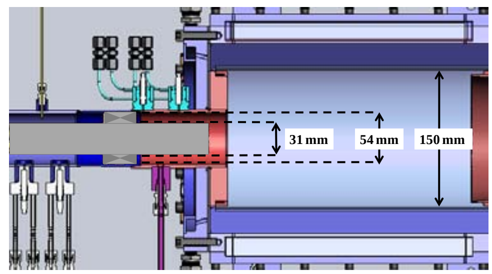

Figure 3 Cross-section view of nozzle and combustion chamber

Operating conditions for the FTF measurements (20 total) presented in this paper are summarized in Table 1. No self-excited instabilities were observed at these operating conditions. For this set of experiments the amplitude of the normalized velocity fluctuation (V'/V_{mean}) was fixed at 5 %.

Table 1 Operating conditions of FTF measurements

P_c [atm]	T_{in} [°C]	V_{mean} [m/s]	φ	P_c [atm]	T_{in} [°C]	V_{mean} [m/s]	φ
1	100	25	0.70	2	200	25	0.65
1	100	30	0.70	2	200	30	0.60
1	100	30	0.75	2	200	30	0.70
1	100	30	0.60	2	200	30	0.65
1	100	35	0.65	2	200	35	0.55
1	200	30	0.70	3	200	25	0.65
1	100	35	0.70	3	200	25	0.60
1	200	35	0.60	3	300	25	0.65
2	100	25	0.60	4	300	25	0.45
2	100	30	0.70	4	300	25	0.50

RESULTS AND DISCUSSION

Effect of Pressure on Stable Flame Structure

Previous research has shown that the flame structure, in terms of shape, length, and flame attachment location, has an effect on the gain and phase of the FTF [7, 8, 20]. Flame length factors into the most common non-dimensional number used to generalize FTF measurements which is the Strouhal number defined as:

$$St = \frac{f * L_{flame}}{V_{mean}} = \frac{L_{flame}}{\lambda_{conv}} \tag{2}$$

In Eq. (2), f is the frequency in Hz, L_{flame} is the flame length in meters, and λ_{conv} is the convective wavelength of the perturbation in meters.

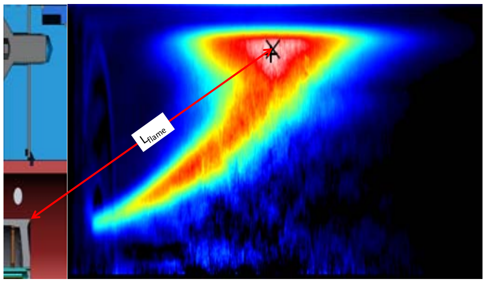

Figure 4 A typical deconvoluted time-averaged chemiluminescence flame image illustrating definition of flame length

A typical deconvoluted time-averaged chemiluminescence flame image is shown in Figure 4. The flow direction is from left to right in the image, and only the top half of the image is shown because the image is axisymmetric. Chemiluminescence intensity is displayed in pseudo color in the image with white being the highest and black the lowest intensity. The flame is inverted conical in shape and the flame length, defined as the distance from the edge of the centerbody to the maximum chemiluminescence intensity location within the flame, marked by an X in Figure 4, is used as the characteristic flame length because it represents the convective path a perturbation travels before interacting with the portion of the flame where the majority of the heat release occurs.

Figure 5 shows a series of deconvoluted time-averaged chemiluminescence images. The color scale of each image is unique to that particular image meaning that intensity comparisons cannot be made between images. The top row corresponds to operating conditions at 2 atm and the bottom row corresponds to the same inlet temperature, mean nozzle velocity, and equivalence ratio at 1 atm combustor pressure. Comparing any two vertical pairings of images it can be seen that the flame length decreases as the combustor pressure increases. Freitag et al. [16] also observed this trend in their experiments. This is similar to the trend observed when increasing equivalence ratio, which can be seen in either the top or bottom row of images going from left to right. At lean conditions, the laminar flame speed increases with increasing equivalence ratio [21] which explains the trend of decreased flame length with increasing equivalence ratio. Due to the fact that flame length also decreases with increasing combustor pressure it is presumed that the flame speed also increases with increasing pressure. Measurements of the effect of pressure on turbulent flame speed do indeed show an increase with increasing pressure [22, 23].

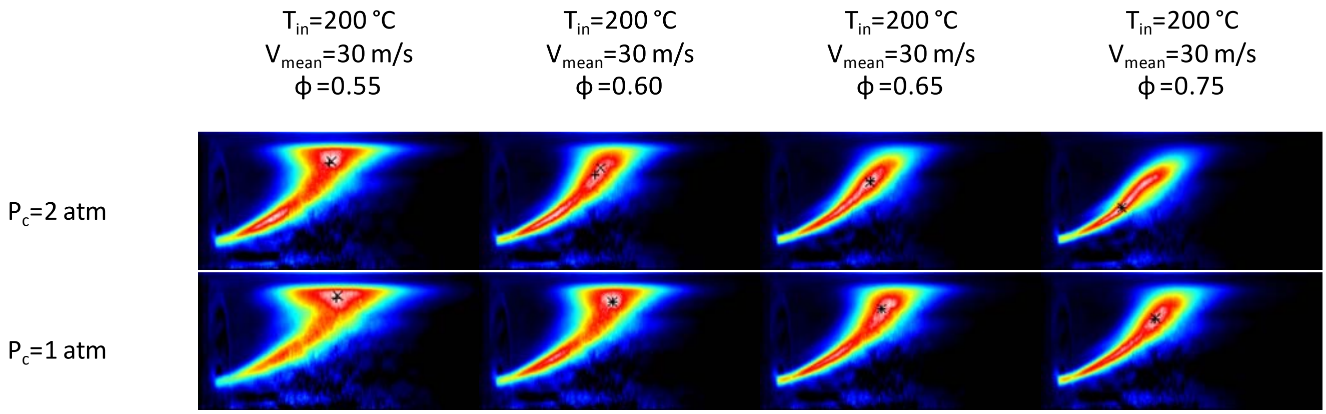

Figure 5 Comparison of stable flame images at 2 atm (top row) and 1 atm (bottom row)

Flame Transfer Function Measurements

A representative FTF gain and phase is plotted in Figure 6. At low frequencies the gain is larger than one and decreases with increasing frequency to a local minimum. Increasing the frequency beyond the first minimum causes the gain to increase to a second maximum. A second region of decreasing gain with increasing frequency then follows. It can be seen that at frequencies where the gain curve shows minima the phase curve shows inflection points. All of the gain and phase curves for the 20 FTF measurements, whose operating conditions are shown in Table 1, exhibit these same characteristics. These characteristics have also been observed in FTF measurements taken by other researchers [6, 9, 24]. Figure 7 shows the gain (top) and phase (bottom) of all 20 measured FTFs plotted against normalized frequency f* [6], which is the frequency divided by the frequency at which the first gain minimum occurs for the particular operating condition. Plotting the gain and phase versus normalized frequency highlights the qualitative similarity, although the actual values of gain and phase do not directly overlap, of all the gain and phase curves across the broad range of operating conditions tested. This suggests that the FTFs measured at elevated combustor pressure are similar to the FTFs measured at atmospheric pressure and in both situations the same mechanism(s) may be responsible for governing the flame's response.

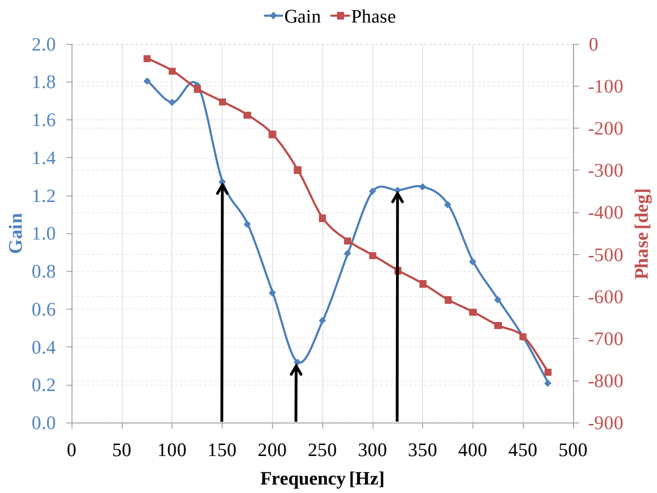

Figure 6 Representative mixture-forced flame transfer function gain and phase versus frequency: P_c=2 atm, T_{in}=200 °C, V_{mean}=30 m/s, φ=0.60, V'/V_{mean}=5 % (arrows indicate frequencies at which phase-synchronized images were taken)

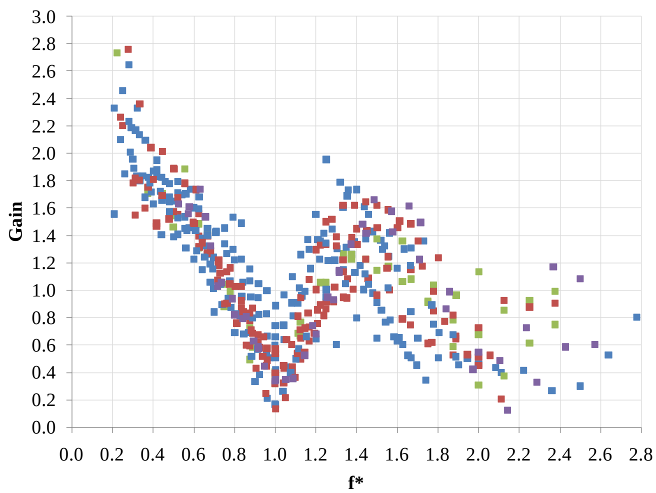

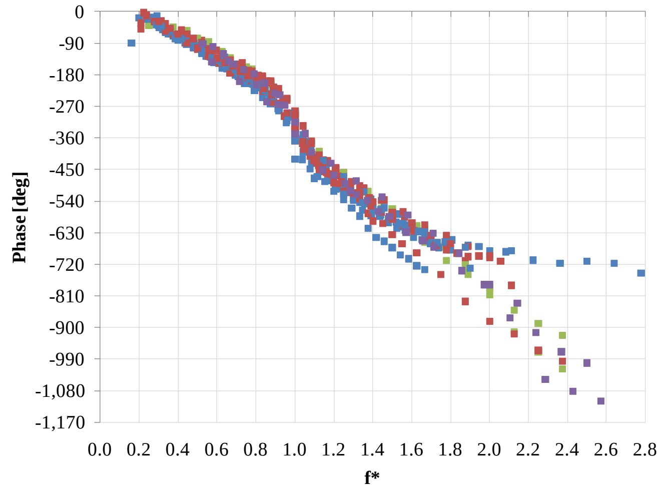

Figure 7 Gain (top) and phase (bottom) of all measured flame transfer functions versus normalized frequency: ■ 1 atm, ■ 2 atm, ■ 3 atm, and ■ 4 atm

Generalization of Flame Transfer Function Measurements

As stated previously, the Strouhal number has been used by numerous researchers [7-9, 20, 25, 26] in an attempt to generalize FTF measurements with varying degrees of success. Plots of the gain and phase versus Strouhal number, Eq. (2), for the same data shown in Figure 7, are presented in Figure 8. It can be seen that the data do not collapse as well when plotted versus Strouhal number as they do when plotted against normalized frequency f*, see Figure 7. Since all of the flames exhibit an inverted conical structure the failure of the Strouhal number normalization cannot be attributed to differences in flame structure as suggested by Kim et al. [20]. The failure of the Strouhal number generalization can be explained by the fact that in the definition of Strouhal number, Eq. (2), only a single convective flame perturbation mechanism is taken into account. The fact that the data do not collapse when plotted against Strouhal number indicates that more than one mechanism plays a role in the flame response. As mentioned in the introduction, researchers have recently proposed that the behavior of the gain is the result of the constructive/destructive interference, dependant on frequency, of two mechanisms perturbing the flame [6, 9]. In the following section the mechanisms that have been proposed and the analysis procedures used to quantify those mechanisms will be described.

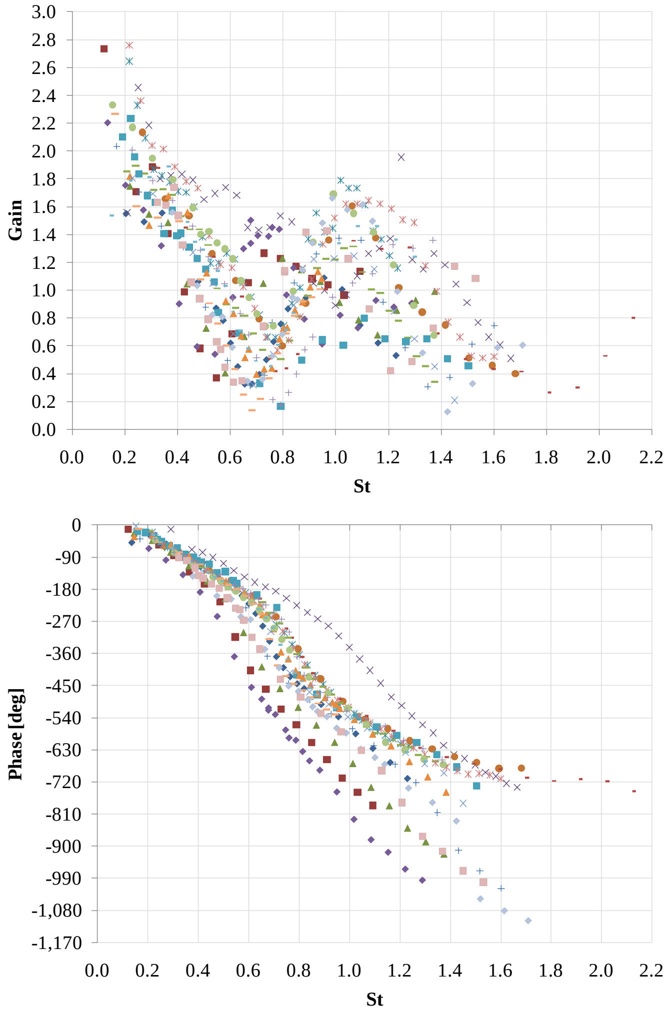

Figure 8 Gain (top) and phase (bottom) of all flame transfer function measurements versus Strouhal number

Flame Response Mechanisms

Palies et al. [9] states that, "The flame is then submitted to a transmitted axial acoustic perturbation which propagates at the speed of sound and to an azimuthal velocity perturbation which is convected at the flow velocity. … The former disturbance induces a shedding of vortices from the injector lip which roll-up the flame extremity while the latter effectively perturbs the swirl number which results in an angular oscillation of the flame root." In order to quantify the relative effects of these two mechanisms on the flame's heat release, phase-synchronized images were taken and analyzed using the following procedure. The flame images were divided into an upper window, where the vortex roll-up should be most evident, and a lower window, where the angular oscillation of the flame root should be most evident. Chemiluminescence intensity was summed in each interrogation window for the series of phase-synchronized images and then plotted against each image's phase angle in the forcing period. At frequencies corresponding to high FTF gain it is shown that the heat release fluctuations in the lower and upper windows are nearly in phase. The opposite is true at frequencies where the FTF gain is low, where the lower and upper window heat release fluctuations are nearly out of phase.

Two different mechanisms are proposed by Jones et al. [6]. They state that, "… the effect of inlet velocity fluctuations can be represented by two separate phenomena. One is the effect of the velocity fluctuation on the mean flame area or mean flame length; while the second is the effect of the vorticity fluctuations generated at the exit of the injector by the inlet velocity fluctuations on local flame wrinkling." Phase-synchronized images are used to quantify the relative contributions of these two mechanisms to the flame's heat release fluctuation. Fluctuations in mean flame area were determined by using a mean flame radius r_m, defined as the radial location of maximum intensity for each axial location in the phase-synchronized image, see Figure 9. An integration of $2\pi r_m$ over the flame was then performed to calculate the mean flame area at each phase. To quantify the effect of vorticity fluctuations a region of the flame whose intensity is greater than 70 % of the maximum intensity is identified for each phase-synchronized image and the radial weighted intensity of this region is summed. These two contributions to the flame's heat release fluctuation are shown to be nearly in phase at frequencies corresponding to high FTF gain and nearly out of phase at frequencies corresponding to low FTF gain.

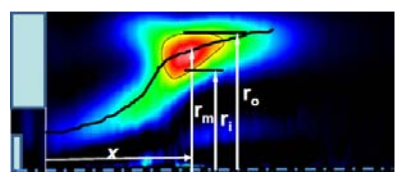

Figure 9 A deconvoluted image with identified mean flame location and center-of-mass region overlaid [6]

In order to assess if these mechanisms are present in this combustor, three series of phase-synchronized images were taken, two at frequencies corresponding to high gain values, 150 and 325 Hz, and one at a frequency corresponding to a low gain value, 225 Hz, at the operating condition presented in Figure 6. The series of deconvoluted flame images at 225 Hz are shown in Figure 10. Two contours are marked within the series of phase-synchronized images. The white contour corresponds to the outer edge of the flame brush from the time-averaged image and the pink contour corresponds to the outer edge of the flame brush for each respective phase. The fact that the two contours overlap in each image indicates that there is no change in the mean flame area over the forcing period. This suggests that the flame length fluctuation mechanism suggested by Jones et al. [6] is not present for this flame. It is also evident from the series of phase-synchronized images that there is no roll-up of the flame tip as seen by Palies et al. [9] in their measurements. Due to the absence of the mechanisms reported in the literature, a new analysis procedure was pursued to identify the cause(s) of heat release fluctuations for this flame.

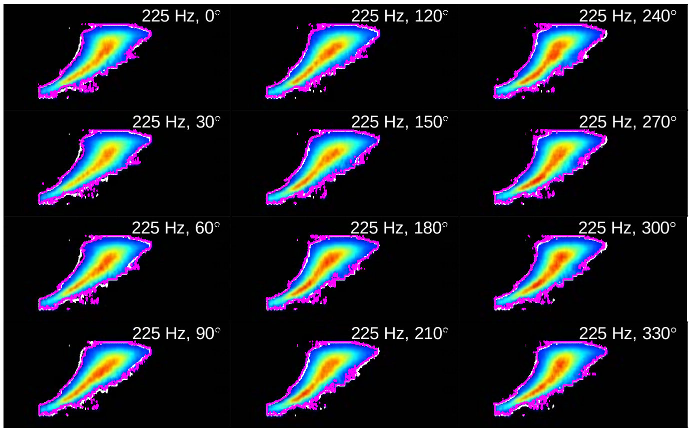

Figure 10 Series of deconvoluted phase-synchronized images at 225 Hz: P_c=2 atm, T_{in}=200 °C, V_{mean}=30 m/s, φ=0.60, V'/V_{mean}=5 %

In a fully premixed flame changes in heat release can be directly correlated to changes in flame surface area [26], and flame surface area can change due to changes in mean flame area and/or due to changes in local flame wrinkling. Therefore if there is a fluctuation in heat release and no change in mean flame area, as is the case for the series of images in Figure 10; the fluctuating heat release must be caused by changes in local flame wrinkling. In order to isolate the fluctuating component of heat release, due to changes in flame wrinkling, the series of phase-synchronized images were analyzed using the technique outlined in Figure 11.

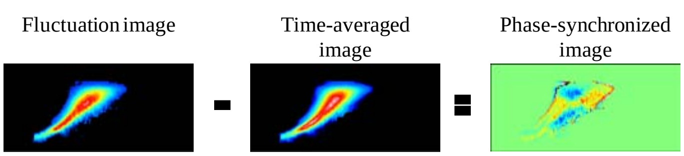

Figure 11 Analysis procedure used to isolate fluctuating component of heat release

The deconvoluted time-averaged image was subtracted pixel by pixel from each deconvoluted phase-synchronized image to obtain what is called a fluctuation image. After the image subtraction process the resulting image is multiplied by 2πr, where r is each pixel's radial coordinate, to account for the fact that these images are a two-dimensional representation of the three-dimensional flame. Fluctuation images show regions within the flame brush where the heat release is either above or below its mean value, denoted by warm and cool colors respectively. Figure 12 shows the series of fluctuation images for the deconvoluted phase-synchronized images shown in Figure 10. Two additional series of fluctuation images which correspond to the other two frequencies, 150 and 325 Hz, marked in Figure 6 are shown in Figure 13 and Figure 14 respectively. In each series of fluctuation images the white contour is again the outer contour of the flame brush from the time-averaged image and the black line is the mean flame radius, r_m, defined similarly to Jones et al [6].

By examining the series of fluctuation images in Figure 12 it can be seen that there are regions of fluctuating heat release above and below the mean flame radius propagating along the flame brush throughout the forcing period. It can also be seen that at any phase the regions of fluctuating heat release above and below the mean flame radius are out of phase, as evidenced by their opposite coloration. The opposite is true of the series of fluctuation images presented in Figure 13 and Figure 14. At any phase in these series of fluctuation images the regions of fluctuating heat release are predominantly of the same color indicating that they are in phase. The qualitative observation regarding the phasing of these regions of fluctuating heat release within the flame brush is quantitatively substantiated by the plots in Figure 15. These plots show the summed heat release fluctuation for the inner and outer regions of the fluctuation images, demarcated by the mean flame radius, as a function of phase. The middle plot shows that the heat release fluctuations at 225 Hz are indeed nearly out of phase and the right plot shows that at 325 Hz the heat release fluctuations are nearly in phase. Examination of the left plot, corresponding to 150 Hz, shows that it is intermediate to the other two frequencies in terms of the phase relationship between the inner and outer heat release fluctuations. This is to be expected because 225 and 325 Hz correspond to absolute minima and maxima respectively in gain whereas 150 Hz is not an extrema and therefore the heat release fluctuations should not be completely in or out of phase, see Figure 6.

The mechanisms that cause these regions of fluctuating heat release ,which then propagate through the flame brush, are the vorticity generated in the inner shear layer, anchored at the tip of the centerbody, and outer shear layer, anchored at the edge of the dump plane, between which the flame is stabilized. Figure 16 shows a snapshot of the vorticity magnitude field in a lean-premixed swirl-stabilized combustor from LES calculations done by Huang and Yang [27]. It can be seen that there are distinct vortices shed from both the centerbody edge and the edge of the dump plane. When these vortices interact with the flame they cause increased flame wrinkling which increases the flame surface area and in turn increases the flame's heat release.

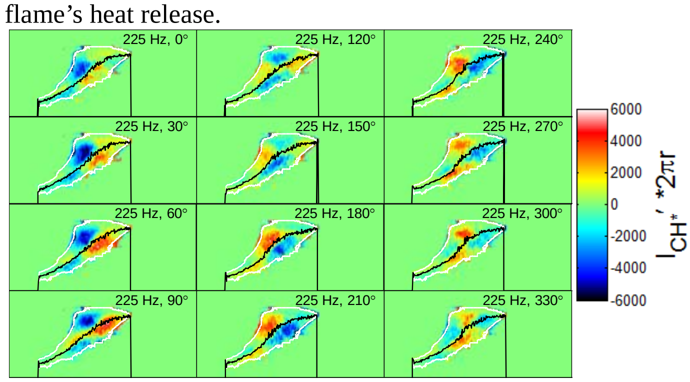

Figure 12 Series of fluctuation images at 225 Hz: P_c=2 atm, T_{in} =200 °C, V_{mean}=30 m/s, φ=0.60, V'/V_{mean}=5 %

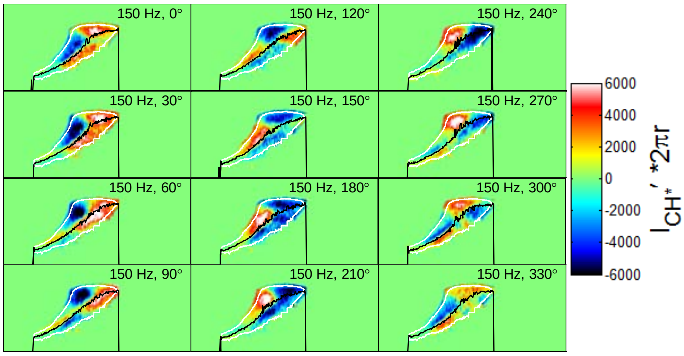

Figure 13 Series of fluctuation images at 150 Hz: P_c=2 atm, T_{in} =200 °C, V_{mean}=30 m/s, φ=0.60, V'/V_{mean}=5 %

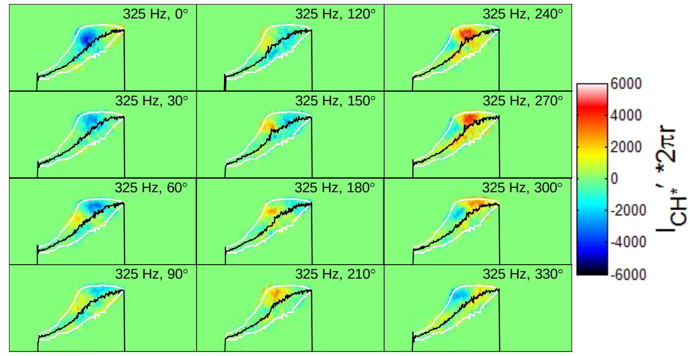

Figure 14 Series of fluctuation images at 325 Hz: P_c=2 atm, T_{in} =200 °C, V_{mean}=30 m/s, φ=0.60, V'/V_{mean}=5 %

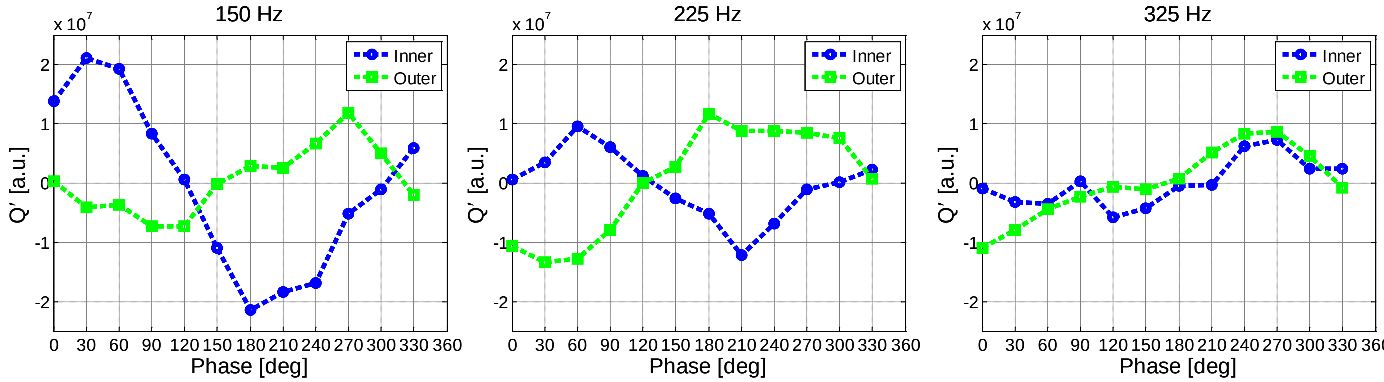

Figure 15 Summed heat release fluctuations in the inner and outer regions, demarcated by the mean flame radius, at 150 Hz (left), 225 Hz (middle), and 325 (Hz) right: P_c=2 atm, T_{in} =200 °C, V_{mean}=30 m/s, φ=0.60, V'/V_{mean}=5 %

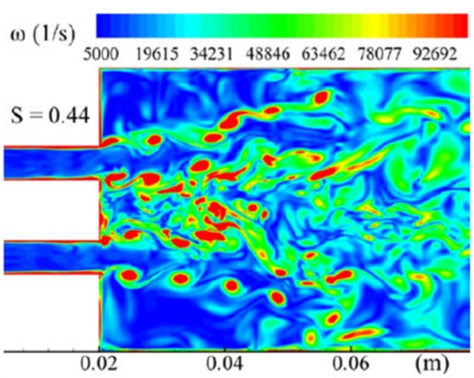

Figure 16 Snapshot of vorticity magnitude field in a lean-premixed swirl-stabilized combustor [27]

CONCLUSION

The mixture-forced flame transfer function of a turbulent, lean fully premixed, swirl-stabilized flame has been measured in an industry scale nozzle over a range of operating conditions encompassing varied combustor pressure, inlet temperature, nozzle mean velocity, and equivalence ratio. All measured FTF gain and phase were found to have qualitative similarity in terms of the shape of the gain and phase curves but quantitative differences in terms of the values of gain and phase. At low frequencies the gain is larger than one, indicating that the flame amplifies low frequency perturbations. As frequency increases the gain decreases to a minimum. Increasing the frequency beyond the first minimum results in the gain increasing to a second peak value. The pattern of a region where gain decreases with increasing frequency followed by a region where gain increases with increasing frequency is then repeated. The magnitude of the phase shows a nearly linear increase with increasing frequency, exhibiting inflection points at frequencies corresponding to minima in the gain.

The fact that the data do not collapse when generalized in terms of Strouhal number indicates that more than one mechanism has an effect on the flame's response. This is because the Strouhal number is defined in terms of only a single convective mechanism. The observed gain behavior is proposed to be the result of constructive/destructive interference of two mechanisms perturbing the flame. Phase-synchronized images were taken to determine if the mechanism pairs proposed by other researchers are present in this experiment. Examination of the phase-synchronized images showed little movement of the flame throughout the forcing period, indicating that heat release fluctuations due to mean flame area changes and those due to vortex roll-up of the flame tip are not present for these experiments.

A new method of analysis for the phase-synchronized images was carried out to isolate the fluctuating component of heat release. These so called fluctuation images highlighted regions of the flame where the heat release was either above or below its mean value. The movement of these regions within the flame was also shown by the fluctuation images. These regions of fluctuating heat release are explained by the vorticity generated in the inner and outer shear layers, between which the flame is stabilized. Vorticity causes changes in flame wrinkling which lead to changes in flame area and ultimately to changes in heat release. At frequencies where the gain is high these vorticity induced heat release fluctuations are found to be in phase leading to an overall amplified flame response. The opposite is true at frequencies where the gain is low and the two heat release fluctuations are found to be out of phase leading to an overall damped flame response.

REFERENCES

[1] Candel, S., 2002, "Combustion Dynamics and Control: Progress and Challenges," Proceedings of the Combustion Institute, **29**, pp. 1-28.

[2] Huang, Y., and Yang, V., 2009, "Dynamics and Stability of Lean-premixed Swirl-stabilized Combustion," Progress in Energy and Combustion Science, **35**, pp. 293-384.

[3] Ducruix, S., Durox, D., and Candel, S., 2000, "Theoretical and Experimental Determinations of the Transfer Function of a Laminar Premixed Flame," Proceedings of the Combustion Institute, **28**, pp. 765-773.

[4] You, D., Huang, Y., and Yang, V., 2005, "A Generalized Model of Acoustic Response of Turbulent Premixed Flame and its Application to Gas-Turbine Combustion," Combustion Science and Technology, **177**, pp. 1109-1150.

[5] Sengissen, A.X., Van Kampen, J.F., Huls, R.A., Stoffels, G.G.M., Kok, J.B.W, and Poinsot, T.J., 2007, "LES and Experimental Studies of Cold and Reacting Flow in a Swirled Partially Premixed Burner with and without Fuel Modulation," Combustion and Flame, **150**, pp. 40-53.

[6] Jones, B., Lee, J.G., Quay, B.D., and Santavicca, D.A., 2010, "Flame Response Mechanisms Due to Velocity Perturbations in a Lean Premixed Gas Turbine Combustor," Proceedings of ASME Turbo Expo 2010, Glasgow, Scotland, UK, June 14-18.

[7] Durox, D., Schuller, T., Noiray, N., and Candel, S., 2009, "Experimental Analysis of Nonlinear Flames Transfer Functions for Different Flame Geometries," Proceedings of the Combustion Institute, **32**, pp. 1391-1398.

[8] Kim, D., Lee, J.G., Quay, B.D., Santavicca, D., Kim, K., and Srinivasan, S., 2008, "Effect of Flame Structure on the Flame Transfer Function in a Premixed Gas Turbine Combustor," Proceedings of ASME Turbo Expo 2008, Berlin, Germany, June 9-13.

[9] Palies, P., Durox, D., Schuller, T., and Candel, S., 2010, "The Combined Dynamics of Swirler and Turbulent Premixed Swirling Flames," Combustion and Flame, **157**, pp. 1698-1717.

[10] Fleifil, M., Annaswamy, A.M., Ghoniem, Z.A., and Ghoniem, A.F., 1996, "Response of a Laminar Premixed Flame to Flow Oscillations: A Kinematic Model and Thermoacoustic Instability Results," Combustion and Flame, **106**, pp. 487-510.

[11] Schuller, T., Durox, D., and Candel, S., 2003, "A Unified Model for the Prediction of Laminar Flame Transfer Functions: Comparisons Between Conical and V-Flame Dynamics," Combustion and Flame, **134**, pp. 21-34.

[12] Lieuwen, T., 2005, "Nonlinear Kinematic Response of Premixed Flames to Harmonic Velocity Disturbances," Proceedings of the Combustion Institute, **30**, pp. 1725-1732.

[13] Preetham, S.H., and Lieuwen, T.C., 2007, "Response of Turbulent Premixed Flames to Harmonic Acoustic Forcing," Proceedings of the Combustion Institute, **31**, pp.1427-1434.

[14] Schuermans, B., Guethe, F., Pennel, D., Guyot, D., and Paschereit, C.O., 2009, "Thermoacoustic Modeling of a Gas Turbine using Transfer Functions Measured at Full Engine Pressure," Proceedings of ASME Turbo Expo 2009, Orlando, Florida, USA, June 8-12.

[15] Cheung, W.S., Sims, G.J.M., Copplestone, R.W., Tilston, J.R., Wilson, C.W., Stow, S.R., and Dowling, A.P., 2003, "Measurements and Analysis of Flame Transfer Function in a Sector Combustor Under High Pressure Conditions," Proceedings of ASME Turbo Expo 2003, Atlanta, Georgia, USA, June 16-19.

[16] Freitag, E., Konle, H., Lauer, M., Hirsch, C., and Sattelmayer, T., 2006, "Pressure Influence on the Flame Transfer Function of a Premixed Swirling Flame," Proceedings of ASME Turbo Expo 2006, Barcelona, Spain, May 8-11.

[17] Waser, M. and Crocker, J., 1984, "Introduction to the Two-microphone Cross-spectral Method of Determining Sound Intensity," Noise Control and Engineering Journal, **22**, pp.76-85.

[18] Lee, J.G., and Santavicca, D.A., 2003, "Experimental Diagnostics for the Study of Instabilities in Lean Premixed Combustors," Journal of Propulsion and Power, **19**, pp. 735-750.

[19] Dasch, C.J., 1992, "One Dimensional Tomography: a Comparison of Abel, Onion-peeling, and Filtered Backprojection Methods," Applied Optics, **31**, pp. 1146-1152.

[20] Kim, K.T., Lee, J.G., Lee, H.J., Quay, B.D., and Santavicca, D., 2009, "Characterization of Forced Flame Response of Swirl-stabilized turbulent Lean-premixed Flames in a Gas Turbine Combustor," Proceedings of ASME Turbo Expo 2009, Orlando, Florida, USA, June 8-12.

[21] Egolfopoulos, F.N., Cho, P., And Law, C.K., 1989, "Laminar Flame Speeds of Methane-air Mixtures under Reduced and Elevated Pressures," Combustion and Flame, **76**, pp.375-391.

[22] Kobayashi, H., 2002, "Experimental Study of High-pressure Turbulent Premixed Flames," Experimental Thermal and Fluid Science, **26**, pp. 374-387.

[23] Liu, C.C., Shy, S.S., Chen, H.C., and Peng, M.W., 2010 "On Interaction of Centrally-ignited, Outwardly-propagating Premixed Flames with Fully Developed Isotropic Turbulence at Elevated Pressure," Proceedings of the Combustion Institute, Article in Press.

[24] Schuller, T., Ducruix, S., Durox, D., and Candel, S., 2002, "Modeling Tools for the Prediction of Premixed Flame Transfer Functions," Proceedings of the Combustion Institute, **29**, pp. 107-113.

[25] Palies, P., Schuller, T., Durox, D., and Candel, S., 2010, “Modeling of Premixed Swirling Flames Transfer Functions,” Proceedings of the Combustion Institute, Article in Press.
[26] Preetham, Santosh, H., and Lieuwen, T., 2008, “Dynamics of Laminar Premixed Flames Forced by Harmonic Velocity Disturbances,” Journal of Propulsion and Power, **24**, pp.1390-1402.
[27] Huang, Y., and Yang, V., 2005, “Effect of Swirl on Combustion Dynamics in a Lean-premixed Swirl-stabilized Combustor,” Proceedings of the Combustion Institute, **32**, pp. 1775-1782.